Available online at www.sciencedirect.com
SCIENCE DIRECT®
Engineering Fracture Mechanics 73 (2006) 1202–1219
Engineering Fracture Mechanics
www.elsevier.com/locate/engfracmech

Effect of material uncertainties on fatigue life calculations of aircraft fuselages: A cohesive element model

P.S. Koutsourelakis [a,*], K. Kuntiyawichai [b], G.I. Schuëller [c]

[a] *Applied Statistics and Economics, Electronics Engineering Technologies Division, Lawrence Livermore National Laboratory, L-227, P.O. Box 808, Livermore, CA 94551, United States*
[b] *Department of Civil Engineering, Faculty of Engineering, Ubonratchathani University, 34190, Thailand*
[c] *Institute of Engineering Mechanics, Leopold-Franzens University, Technikerstrasse 13a, A-6020 Innsbruck, Austria*

Received 11 August 2005; received in revised form 30 December 2005; accepted 2 January 2006
Available online 10 February 2006

Abstract

The present paper deals with the effect of uncertainties on the prediction of fatigue failure of aerospace and mechanical components. Typically the design of such structures has been based on costly experiments or modified versions of Paris' law which are applicable to very restricted range of conditions. The present formulation employs cohesive zone elements in order to resolve the fractured zone in combination with an extrapolation scheme that makes the analysis over hundred of thousands of cycles computationally efficient. The effect of randomness in the cohesive strength is examined with respect to the total lifetime of the specimen.

Keywords: Fatigue; Cohesive elements; Uncertainties; Reliability

1. Introduction

Fatigue is the dominant failure mode in various mechanical components that are subjected to cyclic loading even at stress levels below yielding. Aircraft fuselages and components are typical cases where fatigue failure plays an important role due to the high number of load cycles that they are subjected during their lifetime. Despite the progress in material science and computational mechanics, fatigue life prediction has been based primarily on empirical laws and experimental results. The difficulty in addressing this problem stems from its inherent multi-scale nature. The phenomena associated with fatigue failure transverse multiple length and time scales. On one hand, it has been established that minute flaws in the microstructure (often undetectable by

* Corresponding author. Tel.: +1 925 424 5231; fax: +1 925 422 4141.
E-mail address: koutsourelakis2@llnl.gov (P.S. Koutsourelakis).

0013-7944/$ - see front matter © 2006 Elsevier Ltd. All rights reserved.
doi:10.1016/j.engfracmech.2006.01.003

Nomenclature

T	interface traction
δ	interface separation
K^{u}	unloading tangential stiffness for cohesive law
K^{r}	reloading tangential stiffness for cohesive law
δ_f	characteristic interface separation
T_{c}	ultimate interface traction
δ_{c}	ultimate interface separation
z_n	effective normal separation
z_t	effective tangential separation
t_n	time instant corresponding to the end of the nth loading cycle
θ_n	value of reloading stiffness K^{r} at time t_n

Subscripts

t	tangential component of separation or traction
n	normal component of separation or traction

existing techniques) coalesce and gradually form one or more dominant cracks that ultimately cause the failure of the specimen. On the other hand, the lifetime of the specimen can span over hundreds of thousands or millions of loading cycles.

Typically fatigue prediction has been based on Paris' law [38] and its improvements [1,21,32,16,14]. Although it represents a crude phenomenological model its predictive ability is quite good as long as the conditions of its applicability are met such as small scale yielding, constant amplitude loading and long pre-existing cracks. The latter condition is however rarely encountered in aircraft components which are carefully fabricated and rarely have any flaws consistent with Paris' law. In fact the time for the appearance of the first significant crack can account for the vast majority of their lifetime. Hence, it is particularly important to adopt models that can accurately describe the fracture initiation process as well as the subsequent damage accumulation and crack propagation.

In a continuum mechanics setting, the study of the formation of cracks has probably its roots in the treatise of Hadamard on the propagation of kinematic discontinuities [22,10]. Therein it was first identified that the loss of ellipticity (or hyperbolicity in transient problems) of the elasto-plastic acoustic tensor as the trigger of crack initiation [3,5,27,35]. In a computational implementation a hyperbolicity indicator can be defined as the minimum of the scalar projection of the acoustic tensor [4]. The minimum determines the direction of the surface of the developing discontinuity and by progressing to the point where the hyperbolicity indicator vanishes, the crack tip speed can be determined. The discontinuity can be treated within the extended finite element method, XFEM [13,31] whereby arbitrary discontinuities can be incorporated in the model without remeshing.

Across the discontinuity, a traction-displacement law, i.e. a *cohesive* law, is imposed. The latter contains a softening branch of the interface tractions with respect to the surface separation. Even though the role of this model in [4] is to dissipate energy due to the crack formation, it can be used independently to describe the phenomena of crack initiation and propagation. The idea of cohesive laws [15,2], has been successfully used in a finite element setting by several researchers [48,7,36]. According to this model, fracture is a gradual phenomenon in which separation takes place across an extended crack 'tip' or cohesive zone and is resisted by cohesive tractions. This theory of fracture allows the incorporation into the analysis of well-established fracture parameters such as the spall strength (i.e. the peak cohesive traction) and the fracture energy of the material which is represented by the area under the cohesive traction-separation curve.

Nevertheless, in most studies it is commonly assumed that one or more dominant microcracks preexist in the specimen, and their propagation is monitored through the proposed procedures. Those defects are introduced during material processing, finishing and service and are widely distributed in size and location. They

originate from chemical, thermal, radiant fields, voids or inclusions of second-phase particles that the specimen is inadvertently exposed to during its lifetime. It has been well established that these flaws exhibit tremendous variability in their dimensions (even in specimens of the same material) which can range from 1 nm (i.e. monocrystalline silicon) to 1 mm or greater (i.e. concrete) and occur in both the surface and the bulk. Due to the intricacy of the phenomenon, it appears therefore that a probabilistic model could give a more realistic representation and account for the multiple sources of randomness that are observed in the actual cases. In addition uncertainties can explain the statistical scatter observed in experimental data. Their incorporation in the analysis offers a rational framework for quantifying the reliability and serviceability of those components.

The present paper focuses on the fatigue life calculations using a cohesive zone model (CZM). The details of the model and its finite element implementation are discussed in the following section. Even though it provides an accurate tool, the computational cost required to perform a full analysis over hundreds of thousands or millions of cycles would have been tremendous. A time acceleration procedure is proposed to alleviate this problem in Section 3. Finally an application in the reliability of aerospace components is discussed in the final section where a probabilistic model for the incorporation of uncertainties is also presented. It should be noted that an abbreviated version of the present paper was presented during the 9th International Conference on Structural Safety and Reliability (ICOSSAR2005), Rome, June 2005 [28,29].

2. Cohesive element model

2.1. Triangular cohesive zone model

In the present study, a cohesive zone element model with a Rankine type activation criterion is advocated because it combines sufficient accuracy in the modeling of crack formation and computational efficiency which is an essential requirement when carrying out fatigue life calculations.

Cohesive zone models were pioneered by Dugdale [15] and Barenblatt [2] in order to overcome the contradictions of infinite stresses at the crack tip that classical elasticity predicted. Instead they assumed the existence of a zero-thickness *process zone* which is precursor to the formation of a new crack. The faces of the process zone are gradually separating while finite cohesive tractions develop which tend to resist the formation of the new surface. They eventually reduce to zero upon attainment of a critical separation.

The advent of computers and the explosive progress in finite element technologies gave rise to several applications of the aforementioned concept in fracture modeling, e.g. [25,32,7,48,8]. In a finite element framework, the material is essentially divided into two groups. The bulk material, which sustains no cracking and whose behavior can be described with the usual constitutive laws and the interface or cohesive elements which are located in between the elements discretizing the bulk material. The cohesive elements have zero-thickness and represent the paths for the development and propagation of cracks in the mesh. The normal and tangential separation of the cohesive interfaces give rise to cohesive tractions based on appropriately selected constitutive relations. Several of those have been proposed over the years [40,12,17]. Their common characteristics is the maximum allowable tensile traction (tensile strength) T_c and the fracture energy G_c which represents work expenditure needed for the creation of a crack surface of unit area. It can be defined as $G_c = \int_0^\infty T(\delta)\,\mathrm{d}\delta$ where $T(\delta)$ and δ are the traction and separation across the interfaces of the cohesive element. It should be noted that even though the models that have been proposed are phenomenological, they have significant descriptive power and have shown good agreement with experimental results.

Most of them have been developed for the purposes of describing fracture under monotonic loading conditions. In this case the modeling of the constitutive behavior under unloading has been omitted or it has been assumed to be non-dissipative. In fatigue problems however, where specimens are subjected to cyclic loads, such models would eventually reach a state in which all active cohesive elements will undergo an elastic, non-dissipative deformation cycle and the crack propagation would be arrested. In order to properly model the phenomenon an irreversible loading-unloading rule should be implemented and a stiffness degradation mechanism should be incorporated that adequately accounts for the accumulation of damage that occurs in the specimen under the effect of multiple loading cycles.

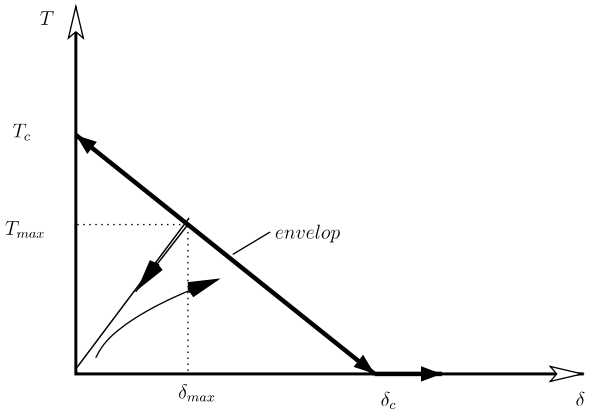

Fig. 1. Constitutive law—normal traction and separation.

Herein the approach of Nguyen et al. [34] is followed and a cohesive law of the form shown in Fig. 1 is used. It is characterized by a small number of parameters and incorporates the aforementioned features which are necessary for modeling fatigue fracture. In particular, the envelop surface is defined by the cohesive strength T_c and the ultimate separation δ_c. Upon attainment of the later it is assumed that the crack has fully formed and the tractions reduce to zero. The cohesive element are activated when the interface traction reaches the critical value T_c. Subsequently they evolve according to the following rate equations: The proposed rate equations for the cohesive forces are:

$$\dot{T}(\delta) = \begin{cases} K^{u}\dot{\delta} & \text{if } \dot{\delta} < 0 \\ K^{r}\dot{\delta} & \text{if } \dot{\delta} > 0 \end{cases} \tag{1}$$

where K^u and K^r are the unloading and loading incremental stiffnesses respectively. The evolution of the later internal variables is governed by the following equations. It is assumed that unloading takes place towards the origin of the T–δ curve and K^u remains constant during this process, i.e.

$$K^{u} = \frac{T_{max}}{\delta_{max}} \tag{2}$$

where T_{max} and δ_{max} are the traction and opening displacement at the point of load reversal respectively. The reloading stiffness K^r is assumed to evolve as follows. For loading, that is for $\dot{\delta} > 0$

$$\dot{K}^{r} = -K^{r}\frac{\dot{\delta}}{\delta_f} \tag{3}$$

where δ_f is a characteristic opening displacement (Fig. 1). For unloading, that is $\dot{\delta} < 0$ it is assumed that $\dot{K}^r = 0$ (constant). K^r is initially (i.e. after the first unloading) set equal to K^u.

The reloading stiffness K^r essentially plays the role of a damage variable and monitors the stiffness degradation due to damage accumulation in the element [44,9]. Its role will be analyzed in detail in the following sections. The parameter δ_f controls the rate of damage accumulation. Larger values of δ_f result in slower degradation of K^r and vice versa.

2.2. Discretized rate equations—integration algorithm

Assume that at time $t = t_n, T_n, \delta_n \in [0, \delta_c], K_n^u, K_n^r$ are known. Given a separation δ_{n+1} at $t = t_{n+1}$, T_{n+1}, the tangential stiffness $dT_{n+1}/d\delta_{n+1}$ and the new values of the internal variables of the cohesive model (K_{n+1}^u, K_{n+1}^r) are obtained. It can be distinguished as the following cases:

- Case A: $\delta_{n+1} \leqslant \delta_n$
  This case corresponds to unloading. Hence from the rate equations above

$$\begin{aligned} K^{\mathrm{u}} &= \frac{T_n}{\delta_n} \\ K^{\mathrm{u}}_{n+1} &= \frac{T_n}{\delta_n} \\ K^{\mathrm{r}}_{n+1} &= K^{\mathrm{r}}_n \\ \dot{T} = K^{\mathrm{u}}\dot{\delta} &\rightarrow T_{n+1} = T_n \frac{\delta_{n+1}}{\delta_n} \\ \frac{\mathrm{d}T_{n+1}}{\mathrm{d}\delta_{n+1}} &= \frac{T_n}{\delta_n} = K^{\mathrm{u}} \end{aligned} \tag{4}$$

- Case B: $\delta_{n+1} > \delta_n$
  This case corresponds to loading. The following subcases are considered:
  (1) Case B.1: $\delta_{n+1} > \delta_{\mathrm{c}}$
  This corresponds to complete loss of the cohesive strength. Therefore:

$$\begin{aligned} T_{n+1} &= 0 \\ \frac{\mathrm{d}T_{n+1}}{\mathrm{d}\delta_{n+1}} &= 0 \\ K^{u}_{n+1} &= K^{\mathrm{r}}_{n+1} = 0 \end{aligned} \tag{5}$$

  (2) Case B.2: $\delta_{n+1} \leqslant \delta_{\mathrm{c}}$
  In this case the reloading stiffness K^{r} evolves as follows:

$$\dot{K}^{\mathrm{r}} = -K^{\mathrm{r}}\frac{\dot{\delta}}{\delta_f} \rightarrow K^{\mathrm{r}}(\delta) = K^{\mathrm{r}}_n \mathrm{e}^{-\frac{\delta-\delta_n}{\delta_f}} \quad \forall \delta \in [\delta_n, \delta_{n+1}] \tag{6}$$

  As for the cohesive traction, two possibilities are considered. Firstly, that the loading curve does not exceed the envelop (Fig. 1). In this case

$$\dot{T} = K^{\mathrm{r}}\dot{\delta} = K^{\mathrm{r}}_n \mathrm{e}^{-\frac{\delta-\delta_n}{\delta_f}}\dot{\delta} \tag{7}$$

  which upon integration leads to

$$T_{n+1} = T_n + K^{\mathrm{r}}_n \delta_f \left(1 - \mathrm{e}^{-\frac{\delta_{n+1}-\delta_n}{\delta_f}}\right) \tag{8}$$

  If T_{n+1} does not exceed the envelop, that is if $T_{n+1} < T_{\mathrm{c}}\left(1 - \frac{\delta_{n+1}}{\delta_n}\right)$ then the calculated stress is accepted. The tangential stiffness $\frac{\mathrm{d}T_{n+1}}{\mathrm{d}\delta_{n+1}}$ is equal to K^{r}_{n+1} (Eq. (6)) and $K^{\mathrm{u}}_{n+1} = T_{n+1}/\delta_{n+1}$.
  On the other hand, if $T_{n+1} < T_{\mathrm{c}}\left(1 - \frac{\delta_{n+1}}{\delta_n}\right)$, then the separation value $\delta_{n+a} \in [\delta_n, \delta_{n+1}]$ where T_{n+a} (Eq. (8)) meets the envelop, has to be determined and subsequently integrate along the envelop in order to find the correct T_{n+1}. Hence the following non-linear algebraic equation has to be solved:

$$T_{n+a} = T_n + K^{\mathrm{r}}_n \delta_f \left(1 - \mathrm{e}^{-\frac{\delta_{n+a}-\delta_n}{\delta_f}}\right) = T_{\mathrm{c}}\left(1 - \frac{\delta_{n+a}}{\delta_n}\right) \tag{9}$$

  For that purpose a Newton–Raphson technique was employed. Once δ_{n+a}, T_{n+a} have been found, we can calculate

$$T_{n+1} = T_{n+a} + (\delta_{n+a} - \delta_{n+1})\frac{T_{\mathrm{c}}}{\delta_{\mathrm{c}}} \tag{10}$$

  From the equation above, we deduce that $\frac{\mathrm{d}T_{n+1}}{\mathrm{d}\delta_{n+1}} = -\frac{T_{\mathrm{c}}}{\delta_{\mathrm{c}}}$. In addition, $K^{\mathrm{u}}_{n+1} = T_{n+1}/\delta_{n+1}$ and K^{r}_{n+1} is given by Eq. (6).
  It should be noted that the integration of the governing equations is exact except for the solution of Eq. (9).

2.3. Activation—pseudo-elastic regime

The implementation of cohesive elements as described above in any finite element software will consist of two basic components modules. The first component has to do with the activation of the cohesive elements and the second with the calculation of their response once they have been activated. A cohesive finite element is activated once the inter-element stress between the adjoining volume elements reaches the critical value T_c. The application of this activation criterion in a finite element software is hindered by several obstacles. Firstly, it is well known that inter-element tractions as calculated do not necessarily have a unique value since different stresses are calculated in each of the adjoining elements. For that purpose smoothing techniques have been developed which alleviate this discrepancy and provide improved estimates of the inter-element tractions. An implementation of such a procedure after each iteration would be very time consuming. Secondly, it would require the definition of global arrays that contain information about the element activation which would need to be passed to all element subroutines. This would be in direct contradiction with the modular structure of existing finite element software.

For those reasons, a relaxed version of the activation criterion above was implemented which uses information on a local level i.e. on each individual cohesive element. In particular, the constitutive law was modified by introducing an artificial elastic branch as seen in Fig. 2. The tangential modulus K_0 was assigned a high value $\frac{(1-\epsilon)T_c}{\delta_c}$ where $\epsilon \ll 1$ (in the applications presented later $\epsilon = 10^{-2}$). The modulus K_0 plays the role of a penalty parameter. Once the element exits the pseudo-elastic regime (i.e. $\delta > \delta_0$), the elastic branch is abolished and the constitutive behavior is governed by the rules presented in the previous section. Despite well-documented numerical instabilities that might arise [19,43], this activation procedure has been selected for its computational efficiency which is crucial to fatigue life calculations.

2.4. Implementation of tangential stiffness

The fundamental ideas of the model presented thus far employ separation and cohesive traction in the normal direction. It is therefore capable of accounting for mode I fracture but nodes for cracking patterns where sliding occurs in the tangential direction. Furthermore, it is reasonable to assume that the sliding separation of the cohesive interfaces affects the normal traction and stiffness degradation and vice versa.

Several models have appeared in the literature that account for this behavior. Most commonly they introduce a normalized measure of separation such as $\delta = \sqrt{\beta^2\delta_t^2 + \delta_n^2}$ [36] where δ_t and δ_n denote the tangential and normal separation and β is a parameter that accounts for the relative influence of the separation modes. This model results in very small tangential stiffness when δ_n or δ_t are close to zero. Herein we propose an

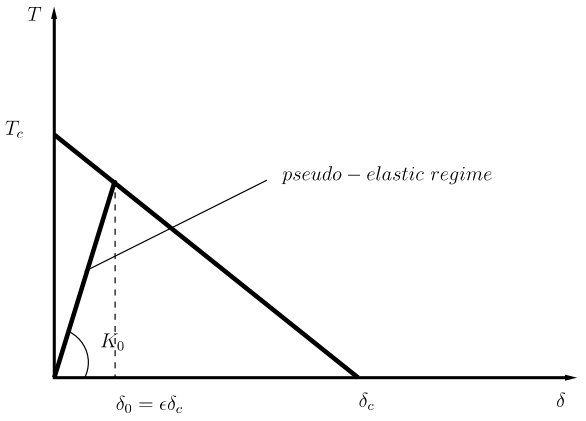

Fig. 2. Relaxed activation criterion.

alternative model in which the normal and tangential cohesive tractions are governed by the same law as the one above but depend on effective measures of normal and tangential displacement, i.e.

$$\text{Effective normal displacement } z_n = \mathrm{e}^{a_t^2\left(\frac{\delta_t}{\delta_{tc}}\right)^2}\frac{\delta_n}{\delta_{nc}}$$

$$\text{Effective tangential displacement } z_t = \mathrm{e}^{a_n^2\left(\frac{\delta_n}{\delta_{nc}}\right)^2}\frac{|\delta_t|}{\delta_{tc}}$$

Evidently the parameters a_t and a_n express the influence of δ_t and δ_n, respectively to the opening separation and sliding. The cohesive tractions T_n and T_t depend on z_n and z_t in the same manner as in the previous models. Hence the rate equations can be expressed as

$$\left(\frac{\dot{T}_n}{T_{nc}}\right) = \begin{cases} K_n^{\mathrm{u}}\dot{z}_n & \text{if } \dot{z}_n < 0 \quad \text{and} \quad z_n > 0 \\ K_n^{\mathrm{r}}\dot{z}_n & \text{if } \dot{z}_n > 0 \quad \text{and} \quad z_n > 0 \\ K_{\mathrm{comp}}\dot{z}_n & \text{if } z_n < 0 \end{cases} \tag{11}$$

$$\left(\frac{\dot{T}_t}{T_{tc}}\right) = \begin{cases} K_n^{\mathrm{u}}\dot{z}_t & \text{if } \dot{z}_t < 0 \\ K_n^{\mathrm{r}}\dot{z}_t & \text{if } \dot{z}_t > 0 \end{cases} \tag{12}$$

The stiffness term K_{comp} is essentially a penalty parameter to prevent negative normal separation i.e. penetration of the cohesive interfaces. One should also note that the effective tangential separation z_t is always positive as it depends on the absolute value of δ_t. The evolution of the reloading stiffness terms K_n^{r} and K_t^{r} follows Eq. (3), i.e. under loading:

$$\dot{K}_q^{\mathrm{r}} = -K_q^{\mathrm{r}}\frac{\dot{z}_q}{z_{qf}} \tag{13}$$

where $q = n$ *or* t and z_{qf} are the characteristic opening displacements that control the rate of stiffness degradation. For unloading, that is $\dot{z}_q < 0$ we assume that $\dot{K}_q^{\mathrm{r}} = 0$ (constant). It is initially (i.e. after the first unloading) set equal to K_q^{u}. The implementation of the proposed cohesive element was done in the general finite element software FEAP [47].

3. Acceleration of fatigue life calculation

The fatigue life of structural elements can reach an exuberant number of cycles. A simulation using cohesive finite elements of the whole lifetime would therefore be computationally infeasible even for quite simplified models with reduced number of nodes and linear elastic constitutive law for the bulk material. In order to alleviate the insurmountable computational load one must sacrifice the accuracy of the calculations. The approximation that is introduced should nevertheless retain the salient features of the deformation process and lead to comparable results with a full analysis.

In the majority of the lifetime analysis, the deformation pattern remains stable and the material stiffness degrades due to the damage accumulated after each cycle. Once the damage level reaches a critical threshold the crack either initiates or propagates further. Hence one can distinguish two time scales: (1) the one in which damage accumulates and stiffness degrades (slow); (2) the one in which the crack propagates. It is conjectured that the damage accumulation process can be modeled intermittently [37]. Following [11], an extrapolation scheme is proposed which avoids the time consuming cycle-to-cycle procedure.

It consists of the following steps:

(1) Perform a detailed simulation for N (i.e. $N = 10$) cycles and record the evolution of the internal variables at the end of each cycle and the state of the system after the last step.
(2) Perform a regression analysis in order to fit an appropriate model for the evolution of each of the internal variables.
(3) Use the fitted model above to extrapolate for the values of the internal variables after M ($M \gg N$) cycles.
(4) Use these values to restart the system assuming $M + N$ cycles have been completed.

It should be noted that once the internal variables of the cohesive elements have been updated, the necessary iterations are performed by the FE code in order to reach the equilibrium state in the full mesh (including the bulk elements).

The proposed procedure has the added advantage that at the restart point, the specimen can be remeshed in order to account for the updated position of the crack tip in which case the internal variables can be appropriately interpolated to obtain the respective values in the new mesh.

3.1. Proposed procedure

In the cohesive model proposed previously, the internal variable that controls the damage accumulation is the reloading stiffness K^{r}. Henceforth we denote it with $\theta_n = K^{\mathrm{r}}(t_n)$ where t_n is end of the nth cycle. Suppose we have obtained with a complete analysis the values $\{\theta_i\}_{i=1}^{N}$. A non-linear evolution law is assumed as follows:

$$\theta_{i+1} = a(\theta_i)\theta_i \tag{14}$$

where $a(\theta) \leqslant 1$ is the reduction factor from cycle i to cycle $i+1$.

Based on the data $\{\theta_i\}_{i=1}^{N}$ we obtain the corresponding $a_i = \frac{\theta_{i+1}}{\theta_i},\ i = 1, \ldots, N-1$ to which we a polynomial model. In the present paper a quadratic polynomial was adopted, i.e. $a(\theta) = c_2\theta^2 + c_1\theta + c_0$, but simpler or more complicated models can also be adopted based on the quality of the fit. The parameters of the model are calculated based on a least-square fit i.e. by minimizing $\sum_{i=1}^{N}(a_i - a(\theta_i))^2$. For the quadratic model this is equivalent to solving the system

$$c_2 \sum_i \theta_i^2 + c_1 \sum_i \theta_i + c_0 \sum_i 1 = \sum_i a_i \tag{15}$$

$$c_2 \sum_i \theta_i^3 + c_1 \sum_i \theta_i^2 + c_0 \sum_i \theta_i = \sum a_i\theta_i \tag{16}$$

$$c_2 \sum_i \theta_i^4 + c_1 \sum_i \theta_i^3 + c_0 \sum_i \theta_i^2 = \sum_i a_i\theta_i^2 \tag{17}$$

Similar systems can be derived for polynomials of any order. Once the proper model has been fitted, it is used to obtain the values of θ at successive cycles.

It should be noted that the reloading stiffness K^{r} of the cohesive elements that have been activated is only being extrapolated.

Furthermore, it was found that the accuracy of the proposed scheme was considerably increased if the time at which a new cohesive element was activated was accurately predicted i.e. it took place during the full analysis of N cycles (step 1). An additional step was therefore implemented in the algorithm. In particular after step 4, a full analysis for one cycle was performed and the number of cohesive elements that were activated up until that point was counted. If that number was considerably different (percentage-wise) from the respective number before the extrapolation then the projection step was reduced by half i.e. $M = M/2$ and the ana-lysis continued from step 3.

3.2. Comparative study of fatigue life calculation

In order to validate the proposed procedure, a comparative study has been carried out between the full fatigue calculations (FFC) and fatigue calculations using the extrapolation algorithm (FCE) described in the previous section. Details of the model used to perform this study are presented in the following.

3.2.1. Geometry of the model (plate with hole under cyclic load)

The material used for this study was 2024-T3 aluminum alloy as the one described in [18]. This alloy has been used in the lower wing skin of many commercial transport aircrafts. The center hole diameter is 6.35 mm. The top and bottom boundary surfaces are subjected to a uniform normal displacement of 0.45 mm. Due to the symmetry of the problem only one quadrant is modeled and appropriate boundary conditions are imposed. Cohesive elements are added to the bottom edge of the model. The cohesive properties are $T_{\mathrm{c}} = 642$ MPa, $\delta_{\mathrm{c}} = 0.0245$ mm. Fig. 3 shows the geometry and FE model.

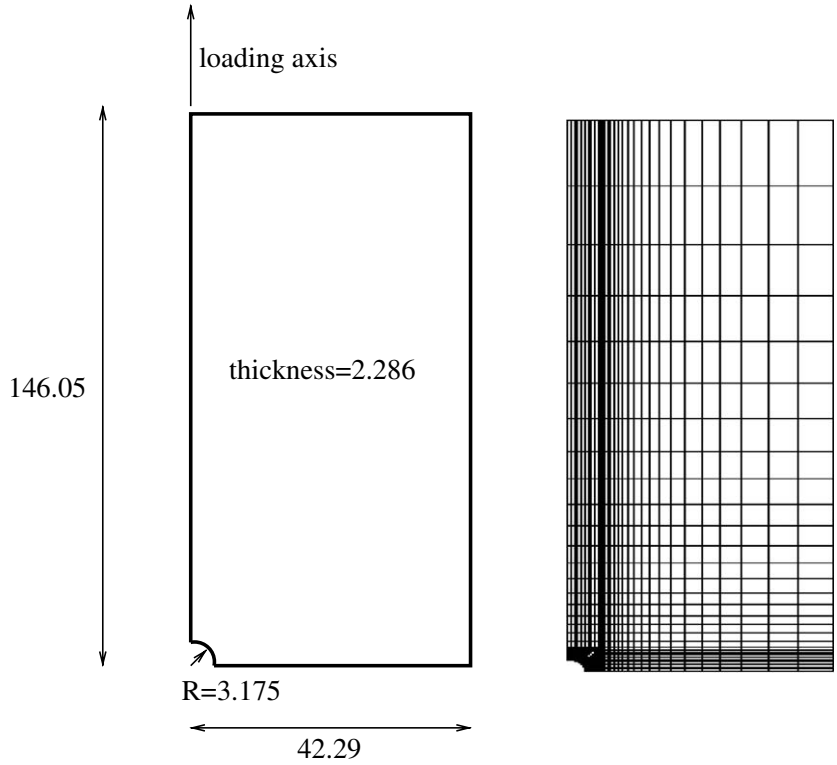

Fig. 3. Geometry of the specimen and finite element model (dimensions in mm).

3.2.2. Material & loading condition

The bulk material was assumed to be elastic–plastic with yield stress, Young's modulus and Poisson ratio equal to 345 MPa, 72 GPa and 0:3, respectively. A cyclic stress with a maximum stress level of 165 MPa (ration $R = -1$) and 0.1 s period was selected and applied at the top edge of the specimen.

3.2.3. Results

In Fig. 4 the crack length time histories obtained with the FFC and FCE method are compared. It can be seen that the agreement is very good. The computational time required using the FFC method was 48 h in contrast to the 43 min needed using the FCE method, i.e. savings of the order of 96% in CPU time.

4. Random field model for cohesive strength

The problem considered herein is motivated by the catastrophic failure of Aloha Airlines Boeing 737 in 1988 due to fatigue cracks emanating from a row of rivet holes on the aircraft fuselage as in Fig. 5 [41,42,20]. The rivet holes constitute locations of stress concentration where multi-site damage can develop and which can lead to the widespread failure of the aircraft's skin. Experimental work has revealed a large scatter in the results and particularly the number of cycles until the ultimate failure [24,33,39]. To this end several researchers have proposed procedures that include the effect of uncertainties in the analysis. Some of them deal with simplified models that neglect recent progress in fracture modeling (see e.g. [6,45]). In some cases even the crack growth process is modeled using stochastic differential equations (see e.g. [30,46]). A common ingredient of the approaches up to date has been the inability to incorporate the crack initiation phase. Most studies assume the pre-existence of a crack and monitor its evolution until failure. In [41,42] for example, the number of cycles until the appearance of initial cracks at the rivet holes were modeled by random variables. Furthermore the cycle numbers for two cracks emanating from the same whole were assumed correlated. The cohesive zone element model however, offers the possibility of modeling fatigue failure *without* the introduc-

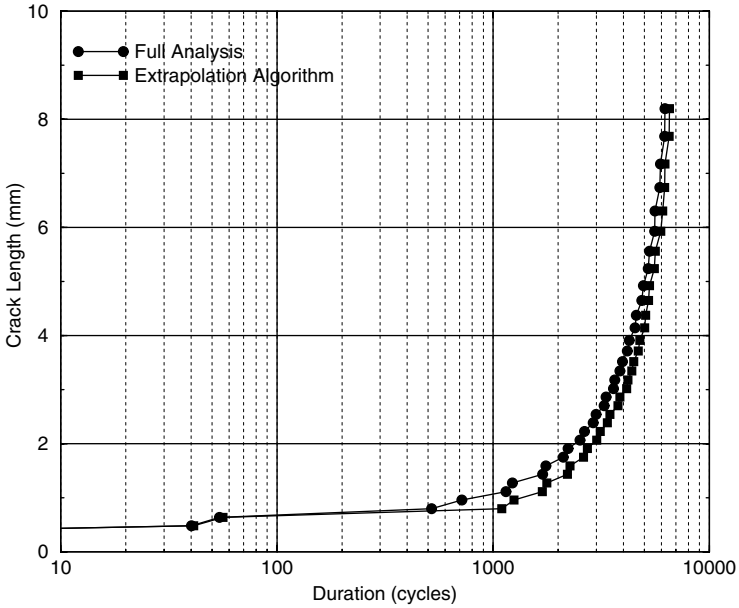

Fig. 4. Comparison of predicted fatigue lifetimes with FFC and FCE.

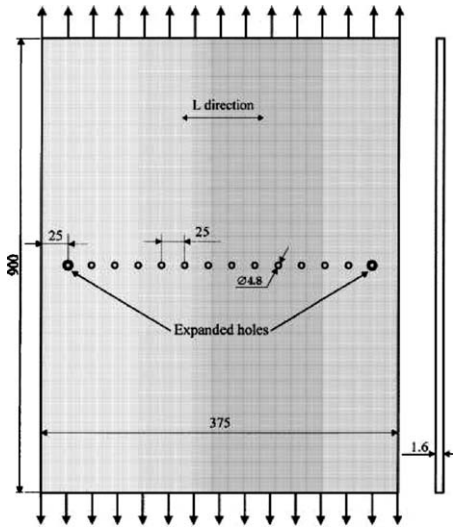

Fig. 5. A row of rivet holes in an aircraft fuselage [26].

tion of initial cracks. As long as the activation criterion of a cohesive element is met, it can account for the damage accumulation that ultimately leads to the formation of a micro-crack. The propagation of that crack can be captured by the rest of the cohesive elements. This is consistent with experimental observations in which no dominant micro-crack or flaw exists (at least it is not visible) in the specimen before it is subjected to cyclic loading.

Assuming no environmental effects which in actual aircrafts might cause flaws to appear [23], it is natural to think that cracks will initiate in areas where the material is weakened during the fabrication process of the component. The weakening of the material might be due to undetectable flaws in the microstructure which eventually coalesce. These areas will certainly be located close to the rivet holes. In the continuum model adopted herein the effect of those micro-flaws will result in a reduced cohesive strength T_c. It is proposed

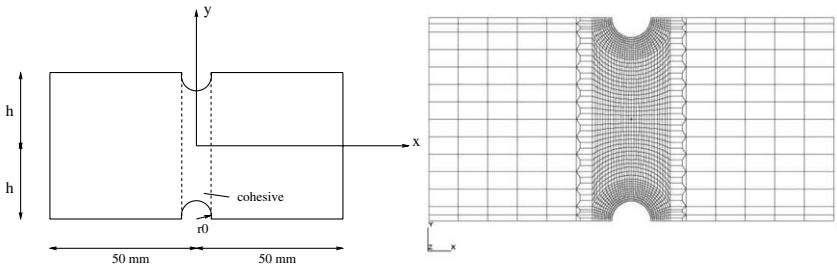

Fig. 6. Configuration and finite element mesh.

therefore to describe the latter parameter with a random field. The following model is not based on actual data which is not available in the literature but rather represents a plausible selection (Due to periodicity, only a part of the row is modeled and the appropriate boundary conditions are imposed (Fig. 6).). For that purpose a statistically inhomogeneous random field $T_c(x,y)$ is selected of the following form:

$$T_c(x,y) = m(x,y) + \sigma \frac{e^{Y(x,y)} - m_y}{\sigma_y} \tag{18}$$

where $m(x,y)$ is the mean field defined below, σ its standard deviation and $Y(x,y)$ a zero-mean, unit variance Gaussian field with isotropic correlation $e^{-(r/b)}$ ($b = 10$ mm). Since the area around the holes is expected to be weaker the following model is proposed for the mean field $m(x,y)$:

$$m(x,y) = \begin{cases} m_1 + (m_2 - m_1)\frac{r - r_0}{r_1} & 2.4 \leqslant r \leqslant r_1 \\ m_2 & r > r_1 \end{cases} \tag{19}$$

where r_0 is equal to 2.4, r is the distance from the center of the closest hole, i.e. if $y > 0$ then $r = h - \sqrt{r_0^2 - x^2}$ and for $y \leqslant 0$, $r = -h + \sqrt{r_0^2 - x^2}$ ($h = 12.5$ mm). The equation above implies that the mean field increases linearly from its minimum value $m_1 = 214$ MPa at the border of the holes to the maximum $m_2 = 642$ MPa which is attained at a distance $r_1 = 5 \times r_0 = 12.0$. The standard deviation σ is taken constant and equal to m_1. Finally it should be noted that parameters $m_Y = e^{0.5}$ and $\sigma_Y = \sqrt{e^2 - e}$ are used for the normalization of e^Y.

Sample realization of the random field $T_c(x,y)$ can be readily generated by simulating samples of $Y(x,y)$ and mapping them according to Eq. (1). It is proposed that each cohesive element is assigned a single value for the cohesive strength which equals the value of $T_c(x,y)$ at the center of the cohesive element. It should be noted that only the central area (indicated by cohesive zone'' in Fig. 6) is modeled with cohesive elements i.e. $-r_0 \leqslant x \leqslant r_0 = 3.4$ mm. The plate dimensions are $50 \times 25 \times 1.6$ mm. The finite element model contained 4724 nodes and 3750 elements in total. Finally the bulk material was modeled as elastic–perfectly plastic with yield stress 345 MPa, Young's modulus 72 GPa and Poisson's ratio 0.3.

5. Numerical results

5.1. Calibration of stiffness degradation parameter δ_f

The parameter δ_f in the cohesive element model controls the rate of stiffness degradation. In the present analysis it is assumed constant everywhere in the mesh. The parameter is phenomenological i.e. it cannot be directly measured in experiments. Hence it must calibrated so that adequate agreement with experimental results is achieved. For that purpose the data contained in [26] seen in Fig. 7 were used.

The data were obtained from tests under imposed stress with constant amplitude of 100 MPa and a ration of $R = 0.1$. Six specimens were tested. The given life expectancies of initiation correspond to the detection of the first crack of a length between 0.5 mm and 1 mm. The evolution of the crack length with the number of loading cycles was measured using an optical microscope.

Specimen Number	Initiation (number of cycles)	Failure (number of cycles)
SMAAC-3.1-AS2-1	125720	200887
SMAAC-3.1-AS2-2	152900	240687
SMAAC-3.1-AS2-3	247000	346687
SMAAC-3.1-AS2-4	179000	283882
SMAAC-3.1-AS2-5	191000	308204
SMAAC-3.1-AS2-6	114870	202021

Fig. 7. Experimental data [26].

It is observed that the experimental data exhibit a large scatter particularly for the crack initiation phase. The calibration of δ_f can be performed using the whole lifetime or just the crack initiation phase. The latter choice was made. In order to deal with the scatter, the mean of the observations which is equal to 166,915 cycles was used as the target value. It was assumed that this value should be reproduced by the mean cohesive element field as shown in Fig. 8.

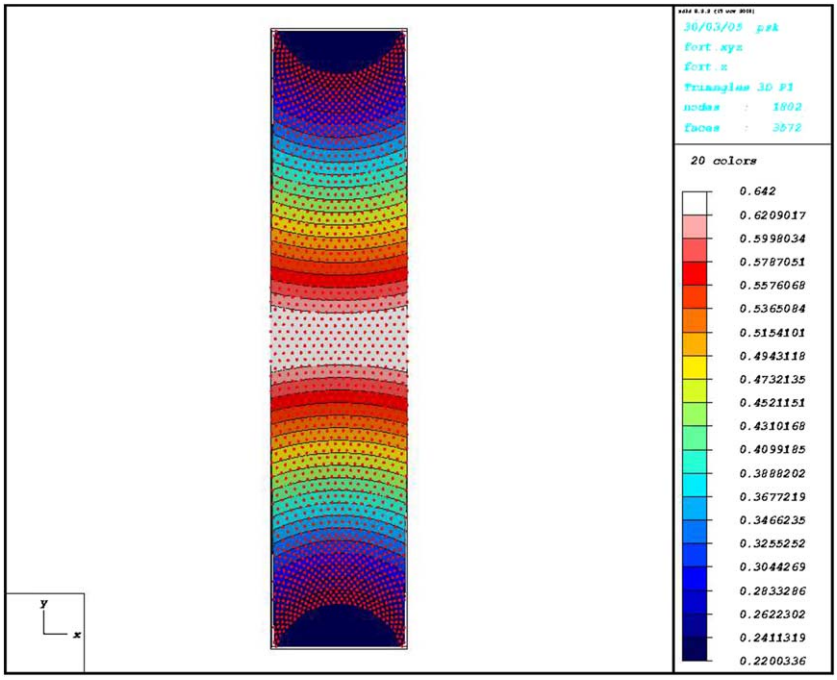

Fig. 8. Contour plot of the mean cohesive strength field.

Based on trial and error, it was found that for $\delta_f = 25$ the resulting crack initiation phase lasted for ~164,000 cycles. This corresponds to the appearance of a first crack of length ~0.8 mm. It is assumed that a crack has fully formed if the tangential reloading stiffness of the respective cohesive element was reduced to 1% of its initial value.

5.2. Effects of material uncertainties on the fatigue life of aircraft fuselage

The model described earlier was used to perform Monte Carlo simulations for various realizations of the cohesive strength T_c. The statistical processing of the results leads to the estimation of the probabilistic characteristics of the lifetime of the specimen. This formulation can account not only for the scatter observed in experiments but also provides a sounder basis for the design of these structures as it allows the assessment of their reliability i.e. the probability of exceeding or not exceeding certain critical levels.

The only difficulty encountered had to do with the computational effort involved as each simulation lasted for 9–12 h on a 2.8 GHz Intel Pentium processor. This precludes the possibility of running a large number of simulations and naturally the results obtained are not very accurate on the low probability region. The accuracy could perhaps be increased by making use of advanced Monte Carlo simulation techniques which will be explored in future studies.

5.3. Discussion of the results

The results obtained are of particular interest as the quantify the effect of uncertainties from the crack initiation phase to the ultimate failure. A histogram of the lifetime of the specimen as estimated based on 227 simulations can be seen in Fig. 9. The probabilities of exceedance for different numbers of cycles are depicted in Fig. 10. The estimated mean value is approximately 343,000 cycles which is fairly close to the experimental mean of 264,000 cycles as seen in Fig. 7. The coefficient of variations is ~0.27 that is considerably larger than the coefficient of variation of the input cohesive strength which ranged from 0.1 close to the rivets to 0.033 far away from them (The coefficient of variation of the experimental results in Fig. 7 is ~0.22.). It should be pointed out that only six experimental samples were available and consequently the confidence in the

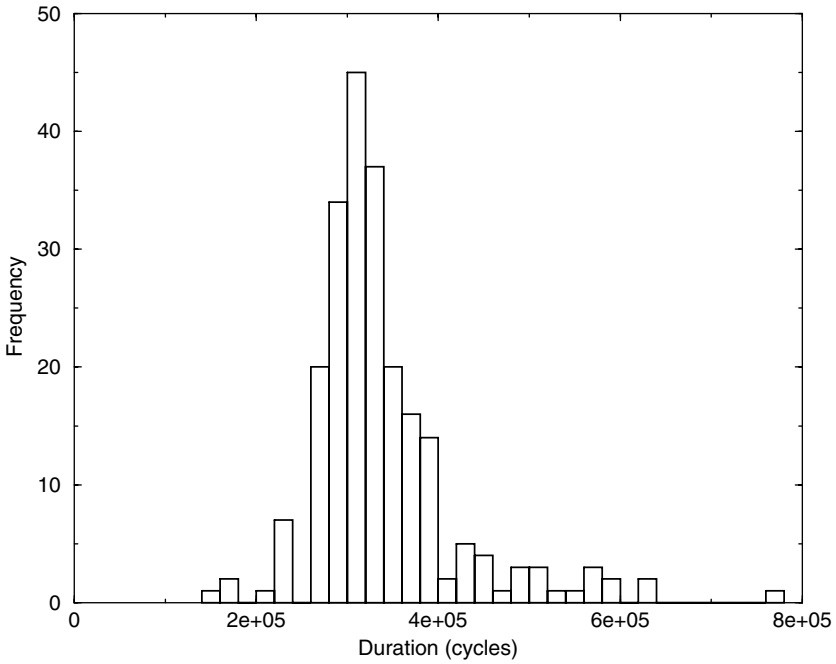

Fig. 9. Histogram of total lifetime.

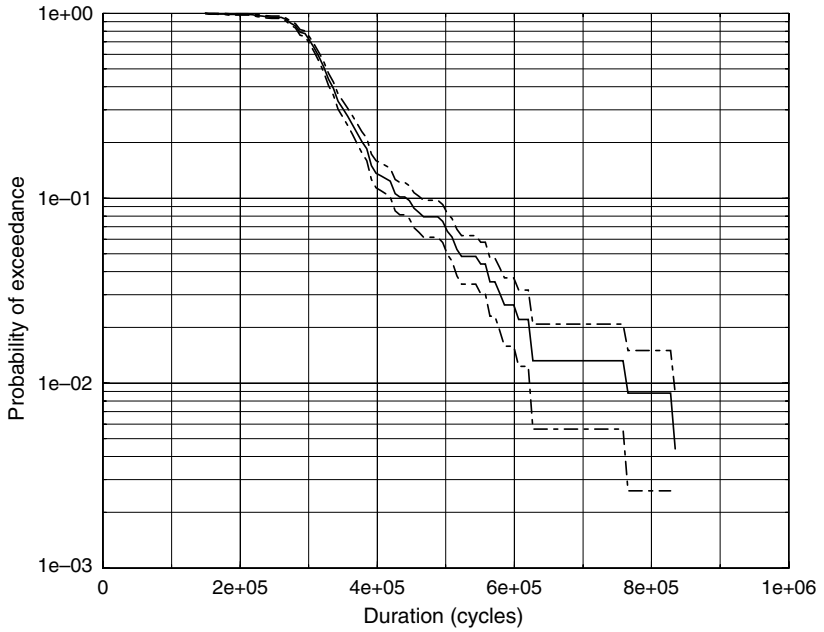

Fig. 10. Probability of exceedance diagram for various durations (dashed lines denote the respective probabilities plus/minus one standard deviations).

respective estimators is rather low. Hence the statistics extracted should be treated with caution and more attention should be paid to the general trends rather than the exact values. The results obtained are summarized in Tables 1 and 2.

- The mean value of 155,565 cycles of the crack initiation phase is in good agreement with the experimental value of 168,415 cycles. However the coefficient of variation is 0.16 in contrast to the 0.29 observed experimentally. Since the initiation phase is determined by the formation of a crack of length of 0.88 mm i.e. by a narrow band of material around the rim of rivets, it seems that the coefficient of variation of the cohesive strength in that area should be larger than 0.1 as considered. A histogram of the duration of crack initiation phase is plotted in Fig. 11.
- The mean and coefficient of variation of the propagation phase (188,245 cycles and 0.41, respectively) are larger than the experimental results of 95,313 cycles and 0.16. Hence, the cohesive strength of the material in the region beyond the rivets is probably less than the value of 642 MPa considered in this study. In

Table 1
Comparison of first and second order statistics (in parentheses experimental results [26])

	Crack initiation phase	Crack propagation phase	Total lifetime
Mean (cycles)	155,565 (168,415)	188,245 (95,313)	343,882 (263,728)
Standard deviation (cycles)	24,324 (48,432)	76792 (14,960)	92140 (59,252)
Coefficient of variations	0.16 (0.29)	0.41 (0.16)	0.27 (0.22)

Table 2
Comparison of cross-correlations between initiation phase, propagation phase and total lifetime (in parentheses experimental results [26])

Crack initiation–crack propagation	Crack initiation–total lifetime	Crack propagation–total lifetime
0.55 (0.65)	0.72 (0.98)	0.98 (0.78)

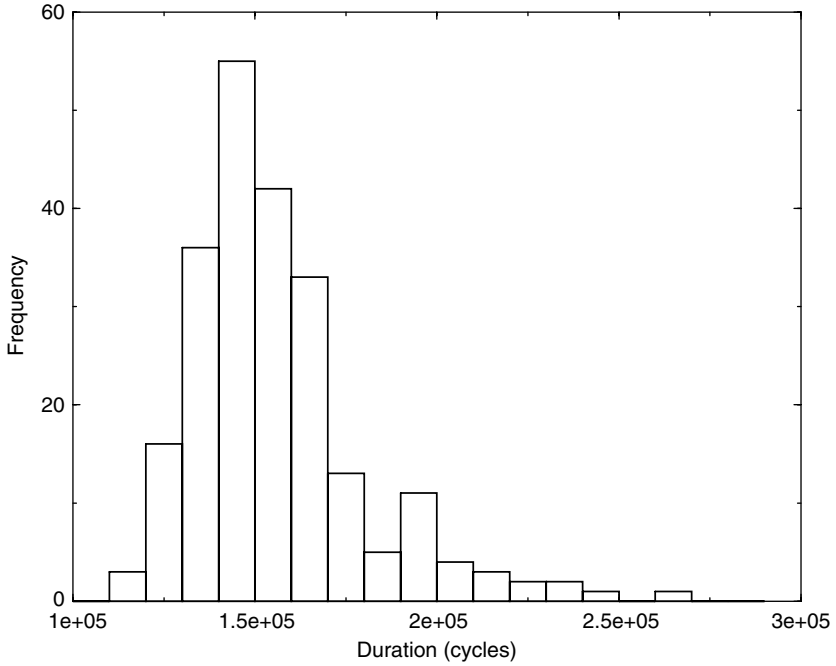

Fig. 11. Histogram of the duration of the crack initiation phase.

addition, the coefficient of variation of T_c is probably smaller. It is reminded that the coefficient of variation of T_c varied linearly from 0.1 at the rivet rim to 0.033 faraway from them. A histogram of the duration of crack propagation phase is plotted in Fig. 12.

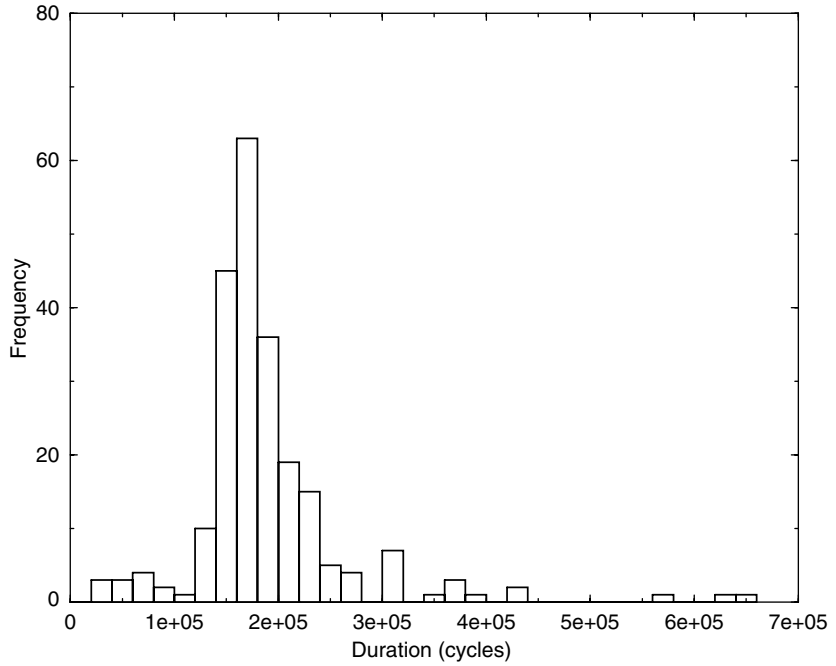

Fig. 12. Histogram of the duration of the crack propagation phase.

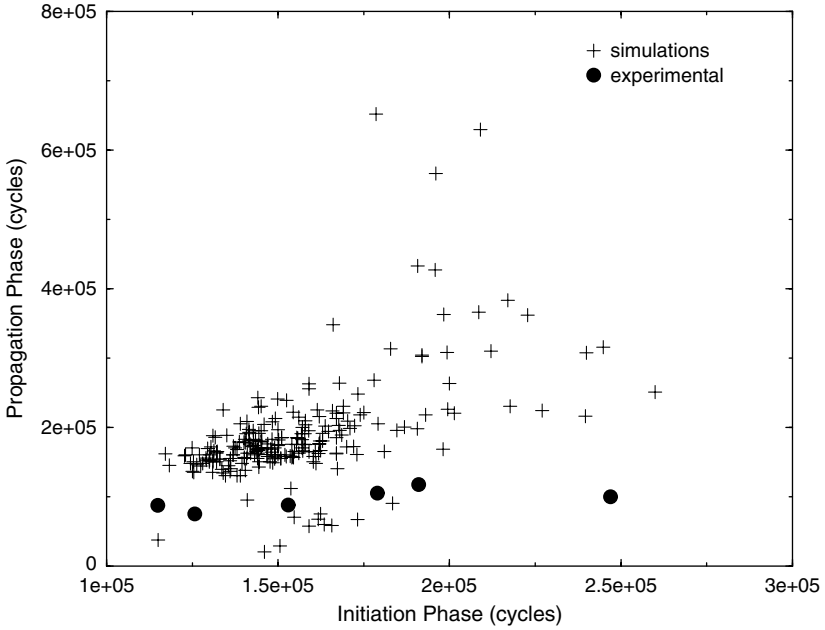

Fig. 13. Scatter plot of the duration of the initiation and propagation phases.

- The aforementioned observations imply that in reality, there is narrow zone around the rivet holes (~1 mm wide) which exhibits reduced cohesive strength due to the fabrication procedure. This zone controls the crack initiation process. Hence in the model of (Eq. (18)), the value of the parameter r_1 should have probably been less than 12 mm and closer to 1 mm or even less. Furthermore m_2 is probably less than 642 MPa.
- Good agreement is also observed in the cross-correlation values between the crack initiation and propagation phase (predicted 0.55 and experimental 0.65), as summarized in Table 2, which emphasizes the qualities of the proposed model. The cross-correlation between the crack initiation and total lifetime of the specimen is 0.72 in contrast to 0.98 observed in the experiments. Hence a strong dependence exists but it is adversely affected by inaccuracies in the prediction of the propagation phase. Similar characteristics are observed in the cross-correlation between the propagation phase and total lifetime (predicted 0.98 and experimental 0.78). A scatter plot of the simulated initiation and propagation times is presented in Fig. 13. As mentioned earlier, the greatest deviation is due to the error in the prediction of the propagation phase.

6. Conclusions

A unified approach which takes into account the effect of material uncertainties in the fatigue life of mechanical components has been presented. Cohesive zone elements have been used in order to model the crack(s) from their initiation to their ultimate length. In order to alleviate the exuberant computational load that is required in order to perform a full analysis over a large number of cycles, an extrapolation scheme for the damage variable has been proposed. It has been demonstrated that sufficient accuracy is retained and significant gains are achieved in terms of computational times. Finally a non-homogeneous random field has been used to model the uncertainties in the cohesive strength, i.e. the fracture properties of the specimen. Due to the lack of experimental measurements for the random variability of the material properties several assumptions had to be made. Nevertheless the results obtained are in good agreement with observations. Most importantly however the present approach quantifies the reliability of the specimen using a unified approach from the crack initiation stage to crack propagation and ultimate failure. Finally, the histograms obtained (not only for the total lifetime but for the initiation and propagation phases) can be used as prior probabilities in a Bayesian framework using actual measurements in order to update the lifetime expectancy or the maintenance schedule.

Acknowledgements

This project was supported by the Austrian Science Foundation (FWF) under the contract P16769-N12. K. Kuntiyawichai acknowledges the financial support from the *Österreichischer Austauschdienst* (*ÖAD*) for joining research at Institute of Engineering Mechanics, Leopold-Franzens University, Innsbruck, Austria, EU.

References

[1] Anderson T. Fracture mechanics: fundamentals and applications. Boca Raton: Boca CRC Press; 1995.
[2] Barenblatt GI. The mathematical theory of equilibrium of cracks in brittle fracture. Adv Appl Mech 1962;7:55.
[3] Bazant Z, Belytschko T. Wave propagation in a strain-softening bar: exact solution. J Engng Mech ASCE 1985;111(3):381.
[4] Belytschko T, Chen H, Xu J, Zi G. Dynamic crack propagation based on loss of hyperbolicty and a new discontinuous enrichment. Int J Numer Methods Engng 2003;58:1873.
[5] Belytschko T, Wang XJ, Bazant Z, Hyun Y. Transient solutions for one-dimensional problems with strain softening. J Appl Mech ASME 1987;54(3):513.
[6] Bertrand G. Risk assessment of damage-tolerant metallic structures. In: Schuëfeller GI, Kafka P, editors. Proceedings of ESREL'99, Munich, Balkema, Rotterdam, September 13–17, 1999. p. 207.
[7] Camacho GT, Ortiz M. Computational modeling of impact damage in brittle materials. Int J Solids Struct 1996;33(20):2899.
[8] Carpinteri A. Mechanical damage and crack growth in slits. Dordrecht, The Netherlands: Martinus Nijhoff; 1986.
[9] Chen CR, Kolednik O, Scheider I, Siegmund T, Tatschl A, Fischer FD. On the determination of the cohesive zone parameters for the modeling of micro-ductile crack growth in thick specimens. Int J Fract 2003;120:517–36.
[10] Dafermos CM. Hyperbolic conservation laws in continuum physics. A series of comprehensive studies in mathematics, vol. 325. Springer; 2000.
[11] de Andrés A, Fernández Alcázar J, López Garcia O. On the use of cohesive interface elements in fracture and fatigue. In: Mang HA, Rammerstorfer FG, editors. Proceedings of the fifth world congress on computational mechanics, Vienna, Austria, volume CD-ROM, July 7–12, 2002.
[12] de Borst R. Numerical aspects of cohesive-zone models. Engng Fract Mech 2003;70:1743.
[13] Dolbow J, Moës N, Belytschko T. An extended finite element method for modeling crack growth with frictional contact. Finite Elements Anal Des 2000;36(3):235–60.
[14] Donahue R, Clark H, Atanmo P, Kumble R, McEvily A. Crack opening displacement and the rate of fatigue crack growth. Int J Fract Mech 1972:209.
[15] Dugdale DS. Yielding of steel sheets containing clits. J Mech Phys Solids 1960;8:100.
[16] Elber W. Fatigue crack closure under cyclic tension. Engng Fract Mech 1970;2:37.
[17] Elices M, Guinea GV, Gómez FJ, Planas J. The cohesive zone model: advantages, limitations and challenges. Engng Fract Mech 2002;69:137.
[18] Everett RA. Jr. The effect of hole quality on the fatigue life of 2024-T3 aluminum alloy sheet. NASA Langley Research Center, NASA-2004-TM212658, 2004. p. 1–15.
[19] Falk ML, Needleman A, Rice JR. A critical evaluation of dynamic fracture simulations using cohesive surfaces. J Phys IV, Proc 2001. Pr–5–43–50.
[20] Foulquier J. Etude du comportement de multifissured sous solicitations cycliques et statiques. Report, Centre Commun de Recherches Aerospatiale, 1996.
[21] Gilbert C, Dauskardt R, Ritchie R. Microstructural mechanisms of cyclic fatigue-crack propagation in grain-bridging ceramics. Ceram Int 1997;23:413.
[22] Hadamard J. Lecons sur la propagation des ondes et les equations de l'hydrodynamique. Paris: Hermann; 2003.
[23] Harlow DG, Wei RP. Probabilities of occurrence and detection of damage in airframe materials. Fatigue Fract Engng Mater Struct 1999;22:427.
[24] Harris CE, Newman JC, Piascik RS, Starnes JH. Analytical methodology for predicting the onset of widespread fatigue damage in fuselage structure. In: Bigelow CA, Hughes WJ, editors. Proceedings of the NAA-NASA symposium on the continued airworthiness of aircraft structures, Atlanta, USA, August 28–30, 1997. p. 63.
[25] Hillerborg A, Modeer M, Peterson P. Analysis of crack formation and crack growth in concrete by means of fracture mechanics and finite elements. Cement Concrete Res 1976;6:773–82.
[26] Kebir H, Roelandt JM, Gaudin J. Monte–Carlo simulations of life expectancy using dual boundary element method. Engng Fract Mech 2001;68:1371.
[27] Klein P, Gao H. Crack nucleation and growth as strain localization in a virtual-bond continuum. Engng Fract Mech 1998;61:21.
[28] Koutsourelakis PS, Kuntiyawichai K, Schuëfeller GI. Effect of uncertainties in fatigue life predictions including the crack initiation phase: a cohesive element model. Technical report, VDI Verlag, 2005.
[29] Koutsourelakis PS, Kuntiyawichai K, Schuëfeller GI. Fatigue life calculations including the crack initiation phase and material uncertainties: a cohesive element model. In Augusti G, Schuëfeller GI, editors. Proceedings of the 9th international conference on structural safety and reliability, CD–ROM, Millpress, Rome, Italy, June 2005.
[30] Lin YK, Wu WF, Yang JN. Stochastic modeling of fatigue crack propagation. In: Eggwertz S, Lind NC, editors. Probabilistic methods in mechanics of solids and structures. Berlin: Springer; 1985. p. 103–10.

[31] Moës N, Dolbow J, Belytschko T. A finite element method for crack growth without remeshing. Int J Numer Methods Engng 1999;46:131–50.
[32] Needleman A. A continuum model for void nucleation by inclusion debonding. J Appl Mech 1987;54(525).
[33] Nesterenko GI. Fatigue and damage tolerance of aging aircraft structures. In: Bigelow CA, Hughes WJ, editors. Proceedings of the NAA-NASA symposium on the continued airworthiness of aircraft structures, Atlanta, USA, August 28–30, 1997. p. 279.
[34] Nguyen O, Repetto EA, Ortiz M, Radovitzky RA. A cohesive model of fatigue crack growth. Int J Fract 2001;110:351–69.
[35] Oliver J, Huespe AE, Samaniego E. On the strong discontinuity approach in finite deformation settings. Int J Numer Methods Engng 2003;56(7):1051.
[36] Ortiz M, Pandolfi A. Finite-deformation irreversible cohesive elements for three-dimensional crack propagation analysis. Int J Numer Methods Engng 1999;44:1267.
[37] Oskay C, Fish J. Fatigue life prediction using 2-scale temporal asymptotic homogenization. Int J Numer Methods Engng 2004;61(3):329.
[38] Paris P, Gomez M, Anderson W. A rational analytic theory of fatigue. The Trend Engng 1961;31.
[39] Pitt S, Jones R. Multiple-site and widespread fatigue damage in aging aircraft. Engng Fract Mech 1997;4(4):237.
[40] Planas J, Elices M, Guinea GV, Gómez FJ, Cendoón DA, Arbilla I. Generalizations and specializations of cohesive crack models. Engng Fract Mech 2003;70:1759.
[41] Proppe C. Probabilistic analysis of multi-site damage in aircraft fuselages. Comput Mech 2003;30:323–9.
[42] Proppe C, Schuëfeller GI. Effects of uncertainties on lifetime prediction of aircraft components. In: Bathe KJ, editor. Proceedings of the first M.I.T. conference on computational fluid and solid mechanics, June 12–14, 2001. M.I.T., Cambridge, MA, USA: Elsevier; 2001. p. 425–8.
[43] Rice JR. Some aspects of crack dynamics. In: Bouchaud E, Jeulin D, Prioul C, Roux S, editors. Physical aspects of fracture (Proceedings of NATO advanced study institute on physical aspects of fracture), June 5–17, 2000. Cargese, Corsica: Kluwer Academic Publishers; 2001. p. 3–11.
[44] Roe KL, Siegmund T. An irreversible cohesive zone model for interface fatigue crack growth simulation. Engng Fract Mech 2003;70:209–32.
[45] Shoji H, Shinozuka M, Sampath S. A Bayesian evaluation of simulation models of multiple-site fatigue cracks. Probab Engng Mech 2001;16:355–61.
[46] Tang J, Spencer BF. Reliability solution for stochastic fatigue crack growth problem. Engng Fract Mech 1989;34(2):419.
[47] Taylor RL. FEAP—A finite element analysis program. UC Berkeley, version 7.5 edition, February 2005.
[48] Xu XP, Needleman A. Numerical simulations of fast crack growth in brittle solids. J Mech Phys Solids 1994;42:1397.